Chapter 9

Vanadium Oxide Thin Films Obtained by Thermal Annealing of Layers Deposited by RF Magnetron Sputtering at Room Temperature

Hernan M. R. Giannetta, Carlos Calaza,
Liliana Fraigi and Luis Fonseca

Additional information is available at the end of the chapter

http://dx.doi.org/10.5772/67054

Abstract

This chapter describes a new deposition method proposed to achieve Vanadium Oxide VO_x/V_2O_5 thin films with high temperature coefficient of resistance (TCR), intended to be used as functional material in IR microsensors (bolometers). The main aim of the work is to attain a deposition method compatible with the lift-off microstructuring technique in order to avoid the use of a reactive-ion etching (RIE) process step to selectively remove the VO_x/V_2O_5 deposited layer in the course of the definition of the bolometer geometry, preventing the harmful effects linked to the spatial variability and the lack of selectivity of the RIE process. The proposed technique makes use of a two-stage process to produce the well-controlled VO_x or V_2O_5 thin films by applying a suitable thermal annealing to a previously deposited layer, which was obtained before at room temperature by RF magnetron sputtering and patterned by lift-off. A set of measurements has been carried out with thin films attained in order to check the quality and properties of the materials achieved with this method. The results reached with V_2O_5 pure phase films are consistent with a charge transport model based on the small polarons hopping derived from Mott's model under the Schnakenberg form.

Keywords: VO_x thin film, V_2O_5 thin film, lift-off compatible, RF magnetron sputtering, thermal annealing, Meyer-Neldel rule, small polaron hopping

1. Introduction

Thin films of materials with high temperature coefficient of resistance (TCR) values are widely used as thermoresistive transducers in uncooled infrared imaging sensors. Mixed Vanadium

Oxide (VO_x) thin films were among the first functional materials chosen for this application due to its simple integration with MEMS technology, which led to the development of the first IR image sensors based on focal plane arrays (FPAs) with thermoresistive transducers in the 1970s–1980s [1]. The main reasons leading to the election of the VO_x thin films as bolometer functional material were its high TCR value (for most commercial devices TCRs are in the range of −2 to –3%/K [2]) and its low 1/*f* noise. First microbolometers were achieved using polycrystalline VO_x mixed oxide thin films, formed by a blend of VO_2, V_2O_3, and V_2O_5 oxide phases, with a thickness of 500–1000 Å, a resistivity of 20kΩ/sq. and a TCR (measured at room temperature) of −2%/K [3]. Since then, numerous works have been published presenting methods to improve the performance of these films and the associated devices. The best balance between the resistivity and the TCR reported for a commercial device was achieved using VO_x thin films with a mixing V−O proportion equal to ($x = 1.8$) [4]. The TCR value of a specific material can be obtained experimentally by measuring the slope of the variation of the film resistivity with the temperature, which is described by the expression TCR = 1/R(dR/dT) [1]. But, as will be shown later, it can be also linked to a material parameter known as the material activation energy ΔW, given by $TCR = -\Delta W/kT^2$ [5], where k is the Boltzmann constant and T the temperature.

Two main methodologies able to control the mixing ratio x of the oxide phases present in the sample have been described in the literature for the experimental synthesis of VO_x thin films. The first one achieves the control of the mixing proportion by using multilayers of pure phase materials. Among the published works based on this method, we can highlight Ref. [6] in which authors were able to control the mixing proportion with a sequence of successive depositions of two known phases, VO_2 and V_2O_5, or Ref. [7] in which authors controlled this ratio with a multilayer of $V_2O_5/V/V_2O_5$. However, the most extended method in literature controls the film-mixing ratio by managing the oxidation rate of the material taken from a pure metallic precursor target (pure vanadium material, 99.9%) used for thin film growth. The deposition process parameters are tuned during the growth cycle to adjust the oxidation rate and, consequently, the ratio of the existing oxide phases that will determine the final thin film properties.

This chapter presents a novel technique to obtain vanadium oxide thin films (VO_x or V_2O_5) using different annealing conditions with starting materials previously deposited and patterned at room temperature. The key objective of the method is to offer compatibility with the lift-off microstructuring technique in order to allow the definition of the bolometer active material geometry without need of a dry etching process. The bolometer functional materials are usually deposited on top of thin dielectric membranes (Si_3N_4/SiO_2) required to accomplish an adequate thermal isolation with respect to the silicon substrate. The thickness and stress level of materials used in this membrane can be crucial for bolometer mechanical stability and a partial etch of these layers during a reactive-ion etching (RIE) step used to conform the active layer (due to an over-etch linked to a spatial variability or a lack of selectivity of the RIE process) can compromise future structure reliability. For that reason, the solution proposed splits the thin film formation into two stages: a first deposition of a precursor thin film on samples with a photoresist layer ready for the lift-off process, obtained from a VO_2 or a metallic V target using RF magnetron sputtering at room temperature; and a second annealing step at a high temperature after the photoresist removal, to promote the oxidation and obtain the desired oxide phase mix required for the application.

http://dx.doi.org/10.5772/67054

The morphological, structural, and optical characterization of the thin films obtained with this method under different annealing conditions were performed using field emission scanning electron microscopy (FE-SEM), X-ray diffraction (XRD), and Raman spectroscopy. The electrical conductivity of the samples was measured as a function of the temperature using a probe station attached to a heated chuck. The DC-conduction data measured for pure phase V_2O_5 thin films was fitted using the Mott's small polaron hopping transport model, taking into account the Schnakenberg phonon distribution model equation. The consistency between the different parameters measured for the V_2O_5 samples processed with the optimal conditions and the assumptions of strong electron-phonon interaction, existence of small polarons, and the nonadiabatic regime for the hopping of charge carriers has been checked, suggesting that small polarons hopping is the main conduction mechanism in pure phase V_2O_5 thin films obtained with this method.

2. Vanadium oxides

Vanadium is a transition metal with a [Ar] $3d^3 4s^2$ electron configuration for the ground state and a centered cubic crystal structure [8]. As a consequence of its multivalent character, it has a number of possible oxidation states (V^{+2}, V^{+3}, V^{+4}, V^{+5}), which form an extensive list of binary V−O systems. Some of them are grouped in the so-called "Magneli phases," with stoichiometric formula V_nO_{2n-1}, and others in the Wadsley phases, with stoichiometric formula V_nO_{2n+1}.

The most commonly used phases, found in various applications due to their particular properties, are the VO, VO_2, V_2O_3, and V_2O_5 oxide phases. Their main characteristics are the following:

VO is one of the many vanadium oxide phases with crystalline cubic structure and good electrical conductivity due to the partially filled conduction band and the delocalization of electrons in the 2 g orbital [9].

VO_2 is an amphoteric compound with the unique property of changing from a semiconductor monoclinic phase to a (semi)metal tetragonal rutile phase at a temperature around 340 K and, therefore, its electrical resistivity together with the optical properties also change up to several orders of magnitude between these two states [10].

V_2O_3 phase, like VO_2 compound, presents an abrupt conductivity change at a temperature around 160 K, evidenced of a metal-insulator transition. In addition, it presents a thermochromic behavior in the infrared band [9].

V_2O_5 is the most stable of all vanadium oxide phases, and the preferred one to be used as thermoresistive material in microbolometer arrays for thermal imaging due to its high TCR value. Vanadium pentoxide is a semiconductor with a bandgap of 2.1–2.4 eV, which presents the following polymorphs: α-V_2O_5 (orthorhombic), β-V_2O_5 (monoclinic or tetragonal), and γ-V_2O_5 (orthorhombic), being the α-polymorph the most stable one [11].

There are many other V−O binary compounds with unique properties beyond the most used ones. A complete guide to the various V=O phases can be found in Ref. [9], including a diagram

that represents the different V−O oxide phases as a function of their oxygen atomic fraction, obtained by thermodynamic calculations.

3. Synthesis of VO_x films

A number of deposition techniques can be highlighted among the different synthesis methods reported in the literature for the synthesis of a multiplicity of Vanadium oxide compounds: sputtering [12], sol-gel process [13], chemical vapor deposition (CVD) [14], pulse laser deposition (PLD) [15], atomic layer deposition (ALD) [9], molecular beam epitaxy (MBE) [16], aqueous solution process [17], and the reactive vacuum evaporation [6].

Nevertheless, to obtain a specific oxide phase, it is necessary to complement one of these deposition methods with a thermal annealing process in order to enhance the crystallinity of the film, as well as to modify its stoichiometry [18]. Two illustrative cases can be found in Refs. [19, 20], where VO_x samples were subjected to a thermal annealing process in air at different temperatures (up to 300°C) and a film recrystallization was detected. Furthermore, it was observed that an increase of the substrate temperature after film deposition promotes the loss of oxygen atoms, which results in a modification of the VO_x film stoichiometry [12].

The temperature conditions required to achieve a particular oxide phase will depend on the enthalpy of formation of the various vanadium oxide compounds [19]. On the basis of the change in the Gibbs free energy associated with each stable Vanadium oxide phase, it can be established that V_2O_5 formation requires temperatures above 434°C, and the stable oxide phases formation sequence will be given in the order: $VO_2 \rightarrow V_2O_3 \rightarrow VO \rightarrow V_2O_5$ [21].

Consequently, it has been necessary to explore the influence of the temperature and the annealing time conditions used in the second step of the proposed thin film growth method in order to establish the optimal set of parameters that lead to attain the desired vanadium oxide phase combination.

3.1. Preparation and synthesis of VO_x films

The sputtering technique, one of the most common physical vapor deposition methods [22], has been the process selected for the growth of vanadium oxide thin films. The key advantages of the sputtering technique over other alternative methods include the resultant film uniformity, the easy scalability to larger substrates, and the high deposition efficiency [23]. There are three main sputtering deposition modes available: DC, RF, and magnetron. The first reported growth of a VO_2 thin film deposited with a reactive sputtering method is typically attributed to Fuls and collaborators, from Bell Telephone Labs in 1967 [24].

A wide range of sputtering process conditions have been reported in the literature for the growth of VO_x thin films with different compositions. The main process parameters that can be customized to control the final composition of the resultant material include the selection of a starting target with a virtually pure precursor material, such as metallic-V [25], VO_2 [12], V_2O_5 [11]; the choice of a specific sputtering deposition method, RF [25] or DC [26];

http://dx.doi.org/10.5772/67054

the alteration of the substrate temperature during the deposition process [27]; the subsequent annealing in vacuum or in an oxidizing atmosphere with a controlled O_2/N_2 ratio [28]; or the application of a varying voltage to the substrate during the deposition [29].

In this work, the conditions explored to achieve the desired vanadium oxide thin films include the use of two different sputtering target materials: VO_2 and metallic-V. The thin films obtained with the sputtering process have been patterned using the lift-off technique, and finally, the samples have gone through a thermal annealing step to obtain the desired film composition. The experimental conditions used for this final annealing step in the case of the metallic-V target have been investigated in order to establish the set of parameters that are required to obtain VO_x and V_2O_5 thin films.

The first step in sample preparation has been the arrangement of a base substrate on which the different layers of vanadium oxide compounds have been deposited. The substrate used has been a Si wafer (100) single-side polished, with a precoating of SiO_2 and Si_3N_4, which has acted as an electrical insulator and as a mechanical buffer layer for subsequent thermal annealing. The surface was subjected to a standard cleanroom cleaning process previously to the deposition.

In order to confirm the compatibility of the proposed growth method with the lift-off microstructuring technique, the vanadium oxide thin films have been deposited on top of substrates partially covered with a photoresist layer. The preparation of the samples starts with the deposition of a layer of TI35E image reversal photoresist (MicroChemicals GmbH) on top of the Si substrates, which is selectively exposed using a photolithographic mask taking advantage of the image reversal feature of the photoresist to obtain negative sidewall profiles adequate for the lift-off process. The photoresist has been finally removed in exposed areas using an AZ developer.

The deposition of the Vanadium oxide thin films has been accomplished by using a BOC Edwards auto 500 Sputtering system, which was equipped with both RF and DC sources, using a maximum substrate temperature of 80°C to avoid damaging the photoresist. A set of vanadium oxide thin film depositions has been conducted under two different conditions.

A first set of samples (labelled as type A) has been obtained from a VO_2 target (brand MCSE, 99.9% purity, 3″ diameter, and 6 mm thick) with the RF source, using a 20 sccm argon flow, a 200 W RF power, and 30 min of deposition time. During deposition, the partial pressure on the chamber was 3.31×10^{-3} mBar, and sample holder was maintained at room temperature.

A second set of samples (labelled as type B) has been obtained from a metallic-V target (brand Kurt J. Lesker, 99.5% purity, 3″ diameter, and 6 mm thick) with the DC source, using a 30 sccm argon and 10 sccm oxygen flow, a 400 W DC power, and 30 min deposition time. During deposition, the partial pressure on the chamber was 6.61×10^{-3} mBar, and sample holder was maintained at 80°C.

Sample preparation was concluded with the lift-off process, which removes the photoresist and the material deposited on top of it with an acetone solvent. At this point, films are ready to endure the thermal treatment required to modify the crystallography and stoichiometry.

Type A samples were subjected to annealing processes using different temperatures: 80, 280, 400, and 475°C and times 8, 6, 4, and 3 h, respectively, in an air atmosphere making use of

an electrical oven with a temperature control. In contrast, with type B samples, it was essential to promote the additional oxidation of the metallic-V and, therefore, all samples were subjected to an annealing process at a higher temperature of 500°C for 30 min, making use of a vacuum oven with a controlled argon/oxygen environment (1 sccm oxygen and 3 sccm argon flow).

After the thermal annealing of the samples, the electrical contacts with the vanadium oxide films were obtained making use of an aluminium metallization in a subsequent process step. The samples resulting from this process sequence are illustrated in **Figure 1**.

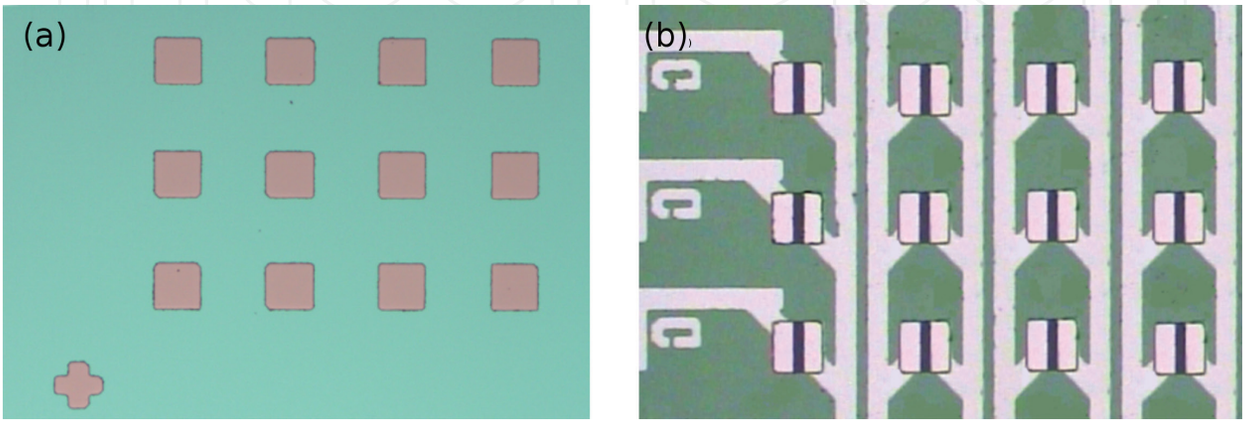

Figure 1. VO_x film conformation by lift-off and metal interconnections: (a) VO_x after lift-off, (b) VO_x with Al metal connections.

4. Characterization of VO_x films

The morphological characterization of the samples has been performed using a field emission scanning electron microscope (FE-SEM, FEI Helios Nanolab 650) with a low acceleration potential, 3 kV. The morphology of the VO_x thin films that result from the proposed growth method is shown in **Figure 2**, with FE-SEM images corresponding to the samples A and B annealed at the highest temperatures, 475 and 500°C, respectively. A good film uniformity can be observed in both the cases as well as in an enhancement of the crystal grain size and shape due to the effect of the thermal annealing [30]. The measured grain sizes are between 100 and 250 nm in both the cases, values that are similar to those reported in the literature for similar materials [31].

The structural characterization was performed by X-ray diffraction (XRD), using a CuKa cathode = 1.5406 Å (XRD-Philips PW 1730/10) configured in a standard Bragg-Brentano powder diffraction geometry. The analysis of the peak coincidences for each sample was performed using the PDF2 database with license from the International Center for Diffraction Data (ICDD). The crystalline phases present in the different samples were determined after the identification of the peak coincidences in the XRD patterns. The most significant results have been obtained for samples annealed at highest temperatures, A@475 and B@500, due to the presence of the dominant V_2O_5 phase, as shown in **Figure 3**.

http://dx.doi.org/10.5772/67054

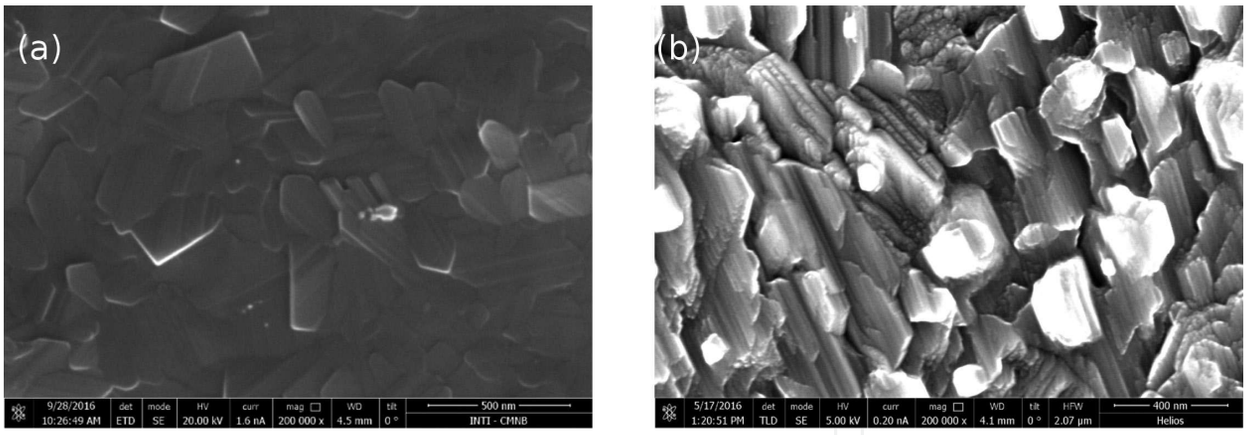

Figure 2. Microscopy Image performed by FE-SEM: (a) sample A@475°C, (b) sample B@500°C.

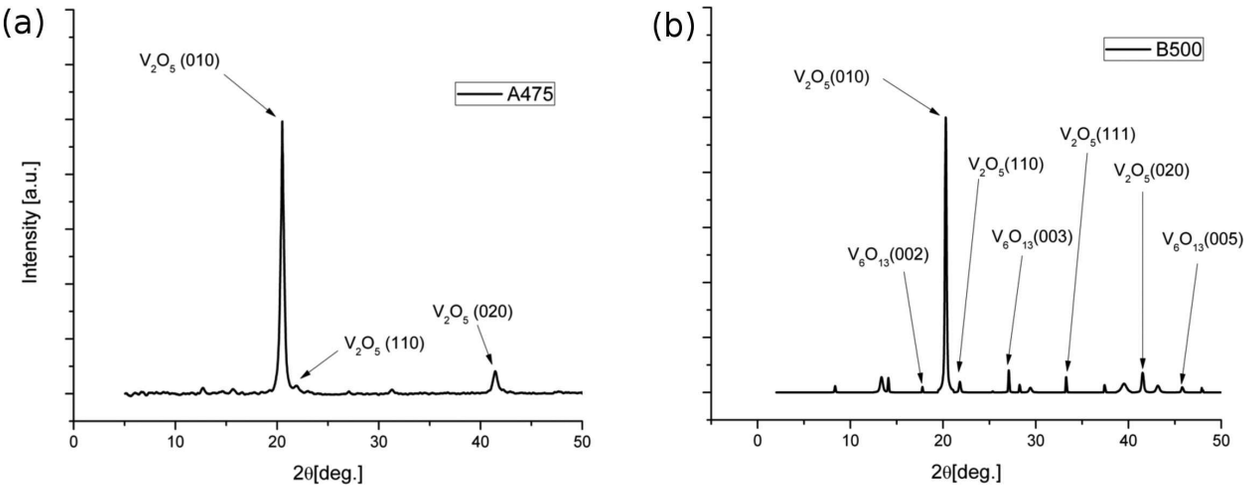

Figure 3. XDR peak matching analysis: (a) sample A@475°C, (b) sample B@500°C.

The analysis of the diffractogram corresponding to A@475 sample shows the presence of a practically pure V_2O_5 oxide phase. Peaks identified correspond to V_2O_5 reflection planes V_2O_5 (010) = 20.25°, V_2O_5 (110) = 21.72°, and V_2O_5 (020) = 41.22°.

In contrast, the presence of a mixed oxide phase can be observed on the diffractogram corresponding to B@500 sample, where main peaks can be attributed to a V_2O_5 phase and secondary ones to a V_6O_{13} phase. The reflection planes identified are V_2O_5 (010) = 20.25°, V_2O_5 (110) = 21.72°, V_2O_5 (111) = 33.27°, V_2O_5 (020) = 41.42°, and V_6O_{13} (002) = 17.77°, V_6O_{13} (003) = 27.08°, V_6O_{13} (005) = 45.78,° and V_6O_{13} (006) = 55.53° for the secondary V_6O_{13} phase.

Optical vibrational modes have been analyzed by means of Raman spectroscopy using a LabRAM HR Raman system (Horiba Jobin Yvon) equipped with a confocal microscope and a charge coupled device (CCD) detector. The 514.5 nm emission line of an Ar + laser has been used as an excitation source. The material databases for peak identification were included in the instrument. The prevailing V_2O_5 phase is once more clearly identified in Raman spectrums obtained for A@475 and B@500 samples due to the perfect matching of the spectrum peaks

with data extracted from the database. **Figure 4** displays the clear correspondence between the measured spectrum for both the samples and the one relative to the V_2O_5 reference material in the database.

The presence of two main emission peaks can be clearly spotted in the Raman spectrum of both samples; a first one in 141.6 cm^{-1}, which corresponds to the V–O–V Raman vibration mode and a second one in 993 cm^{-1}, associated with the V=O double-bond vibration mode [32]. In contrast, the strong emission peak observed in the Raman spectrum of A@475 sample (**Figure 4a**), in 520 cm^{-1}, cannot be assigned to any V–O vibration mode and has been related to the silicon crystalline substrate used as a support for the samples.

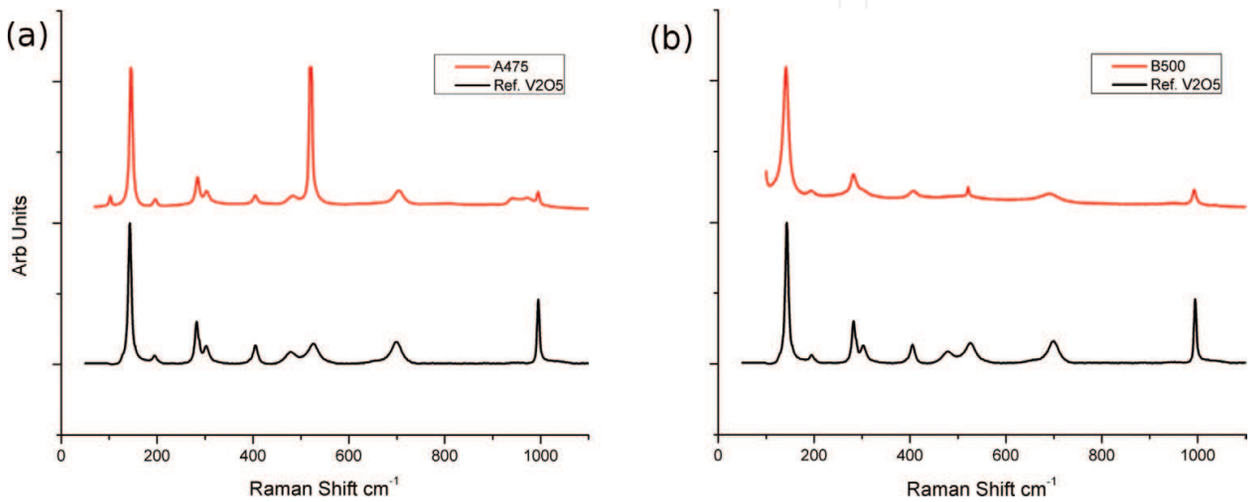

Figure 4. Raman characterization: (a) sample A@475°C, (b) sample B@500°C.

Finally, the electrical conductivity of the Vanadium oxide films has been measured as a function of the sample temperature, using a semiconductor parameter analyser Keithley 4200 CSC connected to a probe station and a thermal chuck equipped with an electronic temperature controller. Resistance measurements were performed using four collinear probes to implement a four-wire measurement scheme. A temperature swept, from room temperature up to 100°C, was applied to the chuck, and the actual temperature achieved by samples was recorded with the help of an additional thermocouple in contact with sample surface.

The measurement of the electrical conductivity as a function of the sample temperature has been used to establish the activation energy corresponding to the different materials by fitting the experimental data with Eq. (1):

$$\sigma_{(T)} = \sigma_0 \exp\left(\frac{-\Delta W}{\kappa T}\right), \tag{1}$$

where σ_0 is a constant, ΔW is the activation energy, k is the Boltzmann constant expressed in eV/k, and T is the temperature in Kelvin. The activation energy was obtained by fitting the experimental data obtained for the electrical conductivity vs. temperature ($\log(\sigma)$ vs. $1000/T$) to

http://dx.doi.org/10.5772/67054

a linear expression derived from Eq. (1) using the least squares method (**Figure 5**). Such linear fits over the experimental measurements provide activation energy values of $\Delta W = 0.267$ eV for the A@475 sample, and $\Delta W = 0.056$ eV for the B@500 sample.

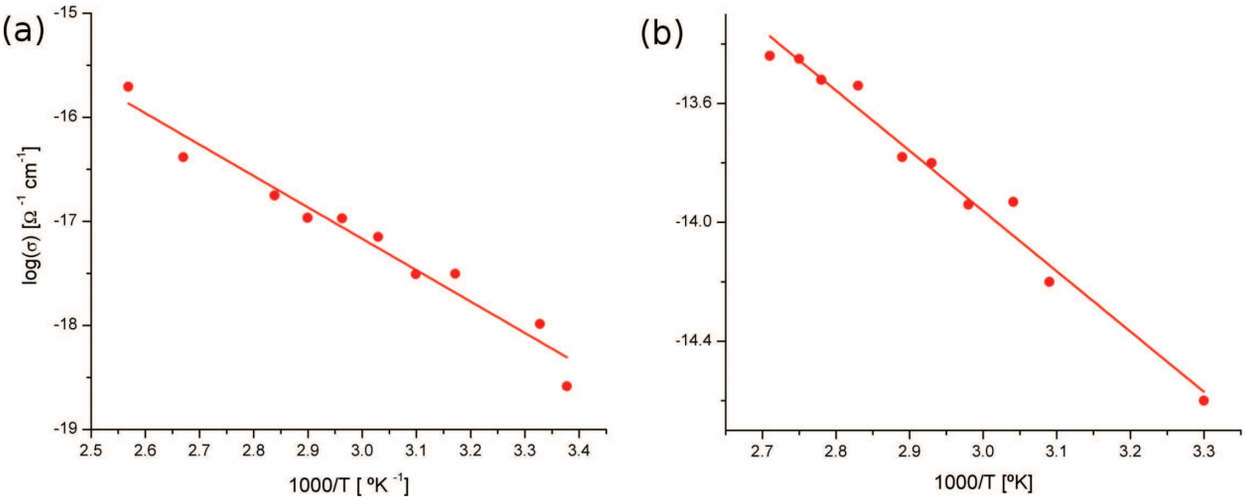

Figure 5. Electrical characterization of samples: (a) sample A@475°C, (b) sample B@500°C.

These activation energy values corroborate that A@475 sample presents a single V_2O_5 phase, as it presents an activation energy similar to that reported by Ioffe [33] for the V_2O_5 single-crystal material with a purity of 99%, $\Delta W = 0.27$ eV. In contrast, the activation energy that has been measured for the B@500 sample is much lower due to the presence of other mixed vanadium oxide phases. Consequently, the TCR value will be higher for the A@475 sample than for the B@500 sample, but the higher value of electrical conductivity in B type samples can represent a benefit in terms of the 1/*f* noise. The TCR estimated for each sample from the measured activation energy using the formerly stated equality $TCR = -\Delta W/kT^2$ [5] is $TCR_{A@475} = 3.44\%/K$ and $TCR_{B@500} = 0.72\%/K$, respectively.

5. Electrical charge transport

The different morphological and structural analysis performed with samples A@475 and B@500 has shown that V_2O_5 is the prevailing vanadium oxide phase formed in all samples due to the use of an annealing temperature well above 434°C, but a slightly different behavior has been perceived in electrical conductivity measurements. The morphological tests determine that A@475 sample presents an almost pure V_2O_5 phase, while a set of mixed vanadium oxide phases VO_x has been obtained for all B type samples, even those that have been processed at the highest temperature, 500°C. Nevertheless, even for these B type samples, the clear preponderance of the V_2O_5 phase when compared with other identified oxide phases, as can be seen on the Raman spectrums in **Figure 4**, should be noted.

The electrical behavior measured for the different vanadium oxide samples, illustrated in **Figure 6a**, shows that electrical conductivity (σ) has an Arrhenius behavior as a function of

temperature (T), indicating that electrical conduction in this material is the result of a thermally activated process. A Meyer-Neldel rule (MNR) relationship is found to hold in a wide variety of such activated processes as the electron conduction in extended states, the ionic conduction, or the thermally activated hopping [34–36]. According to the MNR, the prefactor in Eq. (1) (σ_0) and the activation energy (ΔW) are related by Eq. (2), where σ_{00} is a constant and ΔW_{MNR} is the Meyer-Neldel activation energy

$$\log(\sigma_0) = \log(\sigma_{00}) + \frac{\Delta W}{\Delta W_{MNR}}. \quad (2)$$

The activation energies for the processed samples range from 0.093 to 0.217 eV, according to the experimental data obtained for the electrical conductivity, measured in a temperature range between 25 and 100°C. As can be seen in **Figure 6b**, all of them obey the MNR, with a value of $\sigma_{00} = 4.2 \times 10^{-3}\ \Omega^{-1}\ cm^{-1}$ and $\Delta W_{MNR} = 0.9374$ eV, with a goodness of fit $R^2 = 0.8944$.

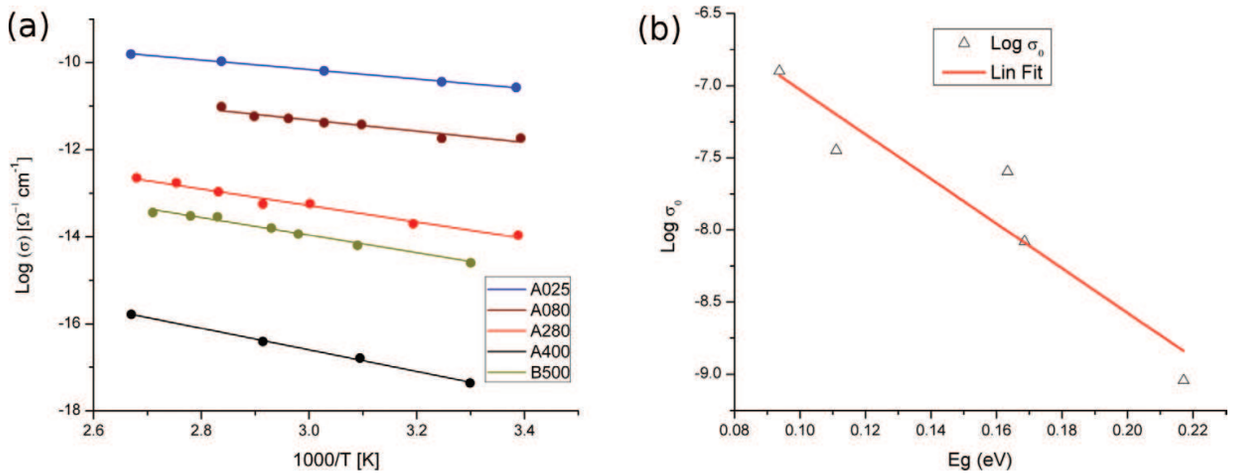

Figure 6. Compliance of activation energy for different processing temperatures with Meyer-Neldel rule: (a) log(σ) vs. 1000/T for samples A and B, (b) fit of ΔW to Meyer-Neldel rule.

The good correspondence observed between the activation energies derived from the electrical conductivity measurements carried out with the different samples and the conventional Meyer-Neldel rule can be attributed to a modification of the location of the Fermi energy level ε_F with respect to the conduction band ε_C with the different annealing conditions applied, similar to the behavior noted in amorphous semiconductors [37].

5.1. Electrical transport in V_2O_5

It is well known that the presence of the V_2O_5 oxide phase is responsible for the high TCR value observed at room temperature in mixed VO_x samples. Small polaron hopping between localized states is the prevailing mechanism that handles the electrical charge transport in the V_2O_5 phase. Mott's works [34, 38] established the basis for the study of this transport mechanisms in transition metals [39], and the proposed models were successively used to experimentally identify this behavior in both single crystal [33] and amorphous V_2O_5 [40] materials. In this section, Mott's models are used to confirm that experimental measurements obtained

http://dx.doi.org/10.5772/67054

with sample A@475, with an almost pure V_2O_5 phase, are consistent with the small polaron hopping charge transport mechanism.

Charge transport through polarons is a well-known effect observed under conditions of strong electron-phonon interaction. One evident effect of strong electron-phonon interaction in a material is the dependence of the electrical conductivity with temperature as seen in analyzed samples. However, other less obvious effect is revealed under this condition, an increase in the effective mass of the electrons due to the interaction with heavy ion nuclei [41]. The assembly formed by the electron and its associated field deformation is known as polaron.

Polarons can be classified taking into account the size of the field deformation radius with respect to the lattice constant, which gives rise to large or small polarons. Charge transport mechanism depends on polaron size; while for large polarons, charges are moved in a unique band, with small polarons, the charge remains trapped on a single ion most of the time. The interaction between the lattice vibration and the localized electron induces charges to jump from one atom to a neighboring one. This process is called conduction by hopping charge carriers and takes place through thermal activation at high temperature [42].

Based on Mott's model, the DC conductivity for the hopping of polarons in a nonadiabatic approximation, above the Debye temperature θ_D is given by Eq. (3) [34, 38]:

$$\sigma = \nu_0 N e^2 R^2 \frac{C(1-C)}{\kappa T} \exp(-2\alpha R) \exp\left(\frac{-\Delta W}{kT}\right), \tag{3}$$

where ν_0 is the optical phonon frequency, N is the number of transition metal ion sites per unit volume, e is the electron charge, α is the wave function decay constant, C is the ratio of ion concentration (V^{+4} vs. V^{+5}), R is the hopping distance, and θ_D is the Debye temperature given by $\theta_D = h\nu_0/k$, where h and k are the Plank and Boltzmann constants. Schnakenberg proposed a simplified model formulation taking into account the phonon distribution [43] in which the dependence of the electrical conductivity with the temperature can be expressed with Eq. (4) [44],

$$\ln(\sigma T) = \ln(\sigma T)_0 - \frac{W_D}{2kT} - \frac{W_H}{kT} \frac{\tanh(h\upsilon_0/4kT)}{h\upsilon_0/4kT}, \tag{4}$$

where σ_0 is a constant, W_D is the activation energy for hopping due to disorder, W_H is the polaron hopping energy, and T the temperature in K. Eq. (4) is valid for the hopping of polarons in the nonadiabatic approximation, above $\theta_D/2$ temperature, where θ_D is the Debye temperature. Total activation energy ΔW can be derived from previous parameters using an expression proposed by Austin-Mott in Eq. (5) [34, 38],

$$\begin{cases} \Delta W = W_H + \frac{W_D}{2} & for\ T > \theta_D/2, \\ \Delta W = W_D & for\ T < \theta_D/4. \end{cases} \tag{5}$$

In order to verify the nature of the electronic transport mechanism in sample A@475, with an almost pure V_2O_5 phase, the experimental data obtained for the electrical conductivity was fitted by using the Mott-Schnakenberg model, as shown in our previous work [45].

The fitting parameters derived by least squares for σ_0, W_H, $W_{D,}$ and $h\nu_0$ have been used to check the condition for polaron existence and to identify the particular type of polaron that is responsible of charge transport. The parameters obtained from the best linear fit, with a 95% confidence interval limits, were W_H = 0.1682 ± 0.0121 eV, W_D = 0.2241 ± 0.0139 eV, and $h\nu_0$ = 0.02755 ± 0.00994 eV; with a goodness of fit R^2 = 0.9827 [45]. The Debye temperature $\theta_D = h\nu_0$/k that corresponds to these values is θ_D = 319 K.

5.2. Verification of the polaron charge transport in V_2O_5

The values extracted for Mott's model parameters with the fit of the electrical conductivity data have been used to check the consistency of the results with the several hypotheses used by Schnakenberg in Mott's model simplified formulation, which involve significant assumptions regarding the transport mechanism. Specifically, we have certified that the strong electron-phonon interaction condition proposed by Austin-Mott, the small polaron formation condition established by Emin-Holstein, the minimum mobility condition for conduction by hopping formulated by Cohen, and the condition proposed by Holstein to set the limit between the adiabatic and nonadiabatic regimes are verified for the temperature range used in measurements.

The strong electron-phonon interaction condition was verified by calculating the ratio of the polaron effective mass m_p to the rigid-lattice effective mass m^*. The higher this ratio, the greater the electron-phonon coupling. The ratio between these two parameters was obtained using Eq. (6) [34, 38],

$$m_p = (\hbar^2/2J\,R^2)\exp(\gamma) = m^*\exp(\gamma), \tag{6}$$

where J is the polaron bandwidth, R is the mean separation between the transition metal ions, and γ is the electron-phonon interaction parameter, which is given by Eq. (7) [34, 38],

$$\gamma = 2\left(\frac{W_H}{h\,\upsilon_0}\right). \tag{7}$$

The condition of small polaron formation was verified using the expression proposed by Emin-Holstein in Ref. [46], an inequality that relates the polaron hopping energy W_H with the bandwidth of the polaron J, as expressed in Eq. (8),

$$J < \frac{W_H}{3}. \tag{8}$$

The bandwidth of the polaron J was estimated from the fitting parameters using the approximate expression proposed by Holstein [47], as shown in the relationship in Eq. (9),

$$J \approx 0.67\,h\,\upsilon_0\,(T/\theta_D)^{1/4}. \tag{9}$$

The type of conduction mechanisms followed by the charge carriers was established using the condition proposed by Holstein [47] to set the limit between the adiabatic and nonadiabatic regimes [34], given by Eq. (10),

http://dx.doi.org/10.5772/67054

$$H = \left(2kT\,W_H/\pi\right)^{1/4}\left(h\upsilon_0/\pi\right)^{1/2}. \tag{10}$$

The polaron conduction regime is determined by the inequality,

$$\begin{cases} J > H & \textit{for} \text{ adiabatic hopping}, \\ J < H & \textit{for non} \text{ - adiabatic hopping}. \end{cases} \tag{11}$$

Finally, for the case of the nonadiabatic regime, the mobility μ has been evaluated using Eq. (11) based on the model proposed by Murawsky [48],

$$\mu = \left(\frac{e\,R^2 J^2}{\hbar kT}\right)\left(\frac{\pi}{4\,W_H kT}\right)^{1/2}\exp\left(-\frac{\Delta W}{kT}\right). \tag{12}$$

Table 1 condenses the values obtained for Mott's model parameters from the fit of the electrical conductivity experimental data achieved with A@475 sample [45], together with the values derived for other parameters using the proposed equations. It can be seen that for temperatures in the range used for measurements (from 25 to 100°C), these values are consistent with the simultaneous verification of the four implicit hypotheses used by Schnakenberg in Mott's model simplified formulation and, therefore, allows us to deduce that the small polarons hopping is the conduction mechanism in V_2O_5 thin films obtained for A@475 samples.

Parameter	Value	Parameter	Value
ΔW	0.2670 eV	J	0.0182 eV
W_H	0.1682 eV	γ	12.2
W_D	0.2241 eV	θ_D	319.7 K
$h\nu_0$	0.0275 eV	μ	1.5×10^{-5} cm^2/Vs

Table 1. Mott's model parameters obtained for V_2O_5 thin films [45].

As a final remark, it is noteworthy that the low value of mobility has been achieved with A type samples, $\mu = 1.5 \times 10^{-5}$ cm^2/Vs. Cohen condition [49] establishes that mobility μ has to be much lower than 10^{-2} cm^2/Vs in the case of a hopping conduction process. This condition was completely met in our V_2O_5 thin film type A samples, with a mobility of $\mu = 1.5 \times 10^{-5}$ cm^2/Vs, while for V_2O_5, monocrystal mobility value of $\mu = 0.15–0.5 \times 10^{-2}$ cm^2/Vs [33] is the limit of Cohen condition.

6. Summary and conclusion

A new method for the preparation of vanadium oxide thin films has been proposed with the aim of providing compatibility with the lift-off microstructuring technique. The thin film

formation has been separated into two phases: a first deposition at low temperature using RF magnetron sputtering and an additional thermal annealing at high temperature to adjust film structure after patterning with the lift-off technique. Different starting materials (sputtering targets) and annealing conditions have been analyzed in order to obtain films with high TCR values for application as infrared microsensors (bolometers).

Samples were analyzed using a variety of characterization techniques comprising SEM, XRD, and Raman. I-V curves were measured in a probe station to establish the dependence of electrical conductivity with the temperature for the different samples.

Structural and optical characterization by XRD and Raman shows that V_2O_5 is the predominant oxide phase identified in all samples, even if mixed phases are observed in samples obtained from the metallic-V target (type B samples).

The electrical characterization showed a negative exponential behavior with temperature for all samples, with an activation energy of 0.267 eV in the case of the pure V_2O_5 phase observed in sample A@475, which corresponds to a TCR value of 3.44%/K.

Regarding the electron transport mechanism in processed samples, it has been found that the electrical conductivity measurements performed with the B type VO_x samples annealed at different temperatures found correlation with a conventional Meyer-Neldel rule, suggesting a thermally activated conduction mechanism.

Finally, it has been found that electrical measurements performed with type A samples, with a pure V_2O_5 phase, are consistent with the electron transport model proposed by Mott for the small polarons hopping. The experimental data was fitted using the Schnakenberg simplified formulation obtaining a polaron hopping energy W_H = 0.1682 eV and an activation energy for hopping due to disorder W_D = 0.2241 eV. The type of charge transport in type A samples was verified by checking the consistency of the resulting fitting parameters with the implicit hypothesis in Schnakenberg formulation: the conditions for the strong electron-phonon interaction, for the existence of small polarons, for the nonadiabatic regime of the hopping of charge carriers, and for the maximum mobility limit. Overall, results suggest that small polarons hopping is the prevalent mechanism driving the electron transport in V_2O_5 thin films obtained with the proposed method.

Acknowledgments

This research leading to these results and chapter edition has been partially funded by the Spanish Ministerio de Economía y Competitividad, through project TEC2013-48147-C6-6-R (TEMINAIR) and supported by grant PRH 2007 No. 203 (PAE 37079), funded by National Institute of Industrial Technology (INTI) and the National Agency for Promotion of Science, Ministry of Science and Technology of Argentina. The authors also wish to thank B. Halac and E. Di Liscia for the Raman spectroscopy, S. Amore for the XRD diffractograms measurements, and L. Patrone for the SEM images performed on samples.

Author details

Hernan M. R. Giannetta[1, 2], Carlos Calaza[3], Liliana Fraigi[1, 2] and Luis Fonseca[3]

*Address all correspondence to: hgiannetta@frba.utn.edu.ar

1 Centro de Micro y Nano Electrónica del Bicentenario (CMNB), Instituto Nacional de Tecnología Industrial (INTI), San Martín, Buenos Aires, Argentina

2 Universidad Tecnológica Nacional (UTN) - Facultad Regional Buenos Aires (FRBA), Argentina

3 Institute of Microelectronics of Barcelona (IMB-CNM, CSIC), Campus UAB, Bellaterra, Barcelona, Spain

References

[1] Kruse P.W., Uncooled Thermal Imaging Arrays, Systems, and Applications. 1st ed. Bellingham, Washington, USA: SPIE; 2001. 90pp. DOI: 10.1117/3.415351

[2] Wang B., Lai J., Li H., Hu H., Chen S., Nanostructured vanadium oxide thin film with high TCR at room temperature for microbolometer. Infrared Physics & Technology, Elsevier. 2013;**57**(03):8–13. DOI: 10.1016/j.infrared.2012.10.006

[3] Wood R.A., Chapter 3. Monolithic silicon microbolometer arrays. In: Kruse P.W. and Skatrud D.D., editors. Infrared Imaging Arrays and Systems. 1st ed. San Diego, CA, USA: Academic Press; 1997. pp. 43–121. DOI: 10.1016/S0080-8784(08)62689-7

[4] Fieldhouse N., Pursel S.M., Horn M.W. and Bharadwaja S.S.N., Electrical properties of vanadium oxide thin films for bolometer applications: processed by pulse dc sputtering. Journal of Physics D: Applied Physics. 2009;**42**(5):055408. DOI: 10.1088/0022-3727/42/5/055408

[5] Jerominek H., Picard F., Vincent D., Vanadium oxide films for optical switching and detection. Optical Engineering. 1993; **32**(9):2092–2099. DOI: 10.1117/12.143951

[6] Subramanyam A., Bharat Kumar Reddy Y. and Nagendra C.L., Nano-vanadium oxide thin films in mixed phase for microbolometer applications. Journal of Physics D: Applied Physics. 2008;**41**(19):195108. DOI: 10.1088/0022-3727/41/19/195108

[7] Han Y.H., Choi I.H., Kang H.K., Park J.Y., Kim K.T., Shin H.J., Moon S., Fabrication of vanadium oxide thin film with high-temperature coefficient of resistance using V_2O_5/V/V_2O_5 multi-layers for uncooled microbolometers. Thin Solid Films, Elsevier. 2003; **425**(1-2):260–264. DOI: 10.1016/S0040-6090(02)01263-4

[8] Shackelford J.F., Han Y.H., Kim S., Kwon S.H., editors. CRC Materials Science and Engineering Handbook. Boca Raton, FL, USA. 4th ed. CRC Publisher; 2015. 634pp.

[9] Bahlawane N., Lenoble D., Vanadium oxide compounds: structure, properties, and growth from the gas phase. Chemical Vapor Deposition, Wiley. 2014;**20**(7–9):299–311. DOI: 10.1002/cvde.201400057

[10] Cardarelli F., editor. Materials Handbook: A Concise Desktop Reference. Springer, London-UK. 2008. ISBN 978-1-4471-3648-4

[11] Zou C.W., Yan X.D., Han J., Chen R.Q. and Gao W., Microstructures and optical properties of β-V_2O_5 nanorods prepared by magnetron sputtering. Journal of Physics D: Applied Physics. 2009;**42**(14):145402. DOI: 10.1088/0022-3727/42/14/145402

[12] Ruzmetov D., Zawilski K.T., Narayanamurti V. and Ramanathan S., Structure-functional property relationships in rf-sputtered vanadium dioxide thin films. Journal of Applied Physics. 2007;**102**(11):113715. DOI: 10.1063/1.2817818

[13] Chae B.G., Kim H.T., Yun S.J., Kim B.J., Lee Y.W. and Kang K.Y., Comparative analysis of VO_2 thin films prepared on sapphire and SiO_2/Si substrates by the sol–gel process. Japanese Journal of Applied Physics. 2007;**46**(2R):738. DOI: 10.1143/JJAP.46.738

[14] Piccirillo C., Synthesis and functional properties of vanadium oxides: V_2O_3, VO_2, and V_2O_5 deposited on glass by aerosol-assisted CVD. Chemical Vapor Deposition. 2007;**13**(4):145–151. DOI: 10.1002/cvde.200606540

[15] Pauli, S.A. and Herger, R. and Willmott, P.R. and Donev, E.U. and Suh, J.Y. and Haglund, R.F., X-ray diffraction studies of the growth of vanadium dioxide nanoparticles. Journal of Applied Physics. 2007;**102**(7):073527. DOI: 10.1063/1.2786917

[16] Rata A.D., Chezan A.R., Haverkort M.W., Hsieh H.H., Lin H.J., Chen C.T., Tjeng L.H. and Hibma T., Growth and properties of strained VO_x thin films with controlled stoichiometry. Physical Review B. 2004;**69**(7):075404. DOI: 10.1103/PhysRevB.69.075404

[17] Takahashi I., Hibino M. and Kudo T., Thermochromic $V_{1-x}W_xO_2$ thin films prepared by wet coating using polyvanadate solutions. Japanese Journal of Applied Physics. 1996;**35**(4A):L438. DOI: 10.1143/jjap.35.l438

[18] Suh J.Y., Lopez R., Feldman L.C. and Haglund R.F., Semiconductor to metal phase transition in the nucleation and growth of VO_2 nanoparticles and thin films. Journal of Applied Physics. 2004;**96**(2):1209–1213. DOI: 10.1063/1.1762995

[19] Melnik V., Khatsevych I., Kladko V., Kuchuk A., Nikirin V., Romanyuk B., Low-temperature method for thermochromic high ordered VO_2 phase formation. Materials Letters. 2012;**68**(1):215–217. DOI: 10.1016/j.matlet.2011.10.075

[20] Fu G., Polity A., Volbers N., and Meyer B., Annealing effects on VO_2 thin films deposited by reactive sputtering. Thin Solid Films. 2006;**515**(4): 2519–2522. DOI: 10.1016/j.tsf.2006.04.025

[21] Xu X., He X., Wang G., Yuan X., Liu X., Huang H., Yao S., Xing H., Chen X. and Chu J., The study of optimal oxidation time and different temperatures for high quality {VO_2} thin film based on the sputtering oxidation coupling method. Applied Surface Science. 2011;**257**(21):8824–8827. DOI: 10.1016/j.apsusc.2011.04.068

[22] Thornton J.A., Plasma-assisted deposition processes: theory, mechanisms and applications. Thin Solid Films. 1983;**107**(1):3–19. DOI: 10.1016/0040-6090(83)90003-2

[23] Nag J. and Haglund Jr R.F., Synthesis of vanadium dioxide thin films and nanoparticles. Journal of Physics: Condensed Matter. 2008;**20**(26):264016. DOI: 10.1088/0953-8984/20/26/264016

[24] Fuls E.N., Hensler D.H., Ross A.R., Reactively sputtered vanadium dioxide thin films. Applied Physics Letters. 1967;**10**(7):199–201. DOI: 10.1063/1.1754909

[25] Schneider K., Lubecka M., Czapla A., VO_x thin films for gas sensor applications. Procedia Engineering. 2015;**120**:1153–1157. DOI: 10.1016/j.proeng.2015.08.1009

[26] Zhang H., Wu Z., Yan D., Xu X., Jiang Y., Tunable hysteresis in metal-insulator transition of nanostructured vanadium oxide thin films deposited by reactive direct current magnetron sputtering. Thin Solid Films. 2014;**552**:218–224. DOI: 10.1016/j.tsf.2013.12.007

[27] Raj, P.D., Gupta S. and Sridharan M., Studies on VO_x thin films deposited over Si_3N_4 coated Si substrates. AIP Conference Proceedings. 2015;**1665**(1):080007. DOI: 10.1063/1.4917911

[28] Tao W., He Y., Xiang D., Ya-Dong J., Chao C. and Ro-Land W., Modeling for VO_2 reactive sputtering process using a pulsed power supply. Chinese Physics B. 2014;**23**(8):088113. DOI: 10.1088/1674-1056/23/8/088113

[29] Kürüm U, Yaglioglu H.G., Küçüköz B., Oksuzoglu R.M., Yıldırım M., Yağcı A.M., Yavru C., Özgün S., Tıraş T. and Elmali A., Modifying ultrafast optical response of sputtered VO_X nanostructures in a broad spectral range by altering post annealing atmosphere. Journal of Optics. 2015;**17**(1):015503. DOI: 10.1088/2040-8978/17/1/015503

[30] Luo Z., Wu Z., Xu X., Du M., Wang T., and Jiang Y., Impact of substrate temperature on the microstructure, electrical and optical properties of sputtered nanoparticle V_2O_5 thin films. Vacuum. 2010;**85**(2):145–150. DOI: 10.1016/j.vacuum.2010.05.001

[31] Chen S., Jianjun L., Jun D., Hong M., Hongchen W., and Xinjian Y., Characterization of nanostructured VO_2 thin films grown by magnetron controlled sputtering deposition and post annealing method. Optics Express. 2009;**17**(26):24153–24161. DOI: 10.1364/oe.17.024153

[32] Benmoussa M., Structural, electrical and optical properties of sputtered vanadium pentoxide thin films. Thin Solid Films. 1995;**265**(1–2):22–28. DOI: 10.1016/0040-6090(95)06617-9

[33] Ioffe V.A. and Patrina I.B., Comparison of the small-polaron theory with the experimental data of current transport in V_2O_5. Physica Status Solidi (b). 1970;**40**(1):389–395. DOI: 10.1002/pssb.19700400140

[34] Austin I.G. and Mott N.F., Polarons in crystalline and non-crystalline materials. Advances in Physics. 1969;**18**(71):41–102. DOI: 10.1080/00018736900101267

[35] Meyer W, Neldel H. Über die Beziehungen zwischen der Energiekonstanten ε under der Mengenkonstantenα in der Leitwerts-Temperaturformel bei oxydischen Halbleitern. [On the relations between the energy constant ε and the quantity constant α in temperature dependent conductivity of oxide semiconductors] Zeitschrift für Technische Physik [J Techn Physics]. 1937;18:588–593.

[36] Yelon A., Movaghar B. and Crandall R.S., Multi-excitation entropy: its role in thermodynamics and kinetics. Reports on Progress in Physics. 2006;**69**:1145. DOI: 10.1088/0034-4885/69/4/R04

[37] Spear W.E., Allan D., Comber P.L., Ghaith A., A new approach to the interpretation of transport results in a-Si. Philosophical Magazine Part B. 1980;**41**(4):419–438. DOI: 10.1080/13642818008245397

[38] Mott N., Conduction in glasses containing transition metal ions. Journal of Non-Crystalline Solids. 1968;**1**(1):1–17. DOI: 10.1016/0022-3093(68)90002-1

[39] Davis E.A. and Mott N.F., Conduction in non-crystalline systems V. Conductivity, optical absorption and photoconductivity in amorphous semiconductors. Philosophical Magazine. 1970;**22**(179):903–922. DOI: 10.1080/14786437008221061

[40] Sanchez C., Morineau R., Livage J. Electrical conductivity of amorphous V_2O_5. Physica Status Solidi (a). 1983;**76**(2):661–666. DOI: 10.1002/pssa.2210760232

[41] Kittel C., editor. Introduction to Solid State Physics. 8th ed. USA: Wiley; 2004. 704pp. ISBN: 978-0-471-41526-8

[42] Devreese J. T., "Polarons" in Encyclopedia of Applied Physics, Vol. 14, pp. 383 – 409. Ed. by G.L. Trigg (VCH, Weinheim, 1996).

[43] Schnakenberg J., Polaronic impurity hopping conduction. Physica Status Solidi (b). 1968;**28**(2):623–633. DOI: 10.1002/pssb.19680280220

[44] Culea E., Gheorghiu, C. and Nicula A., Electrical conductivity of vitreous $75\%V_2O_5 - 25\%(As_2O_3{\cdot}B_2O_3)$, Physica Status Solidi (a). 1986;**96**(1):K85–K88. DOI: 10.1002/pssa.2210960163

[45] Giannetta H.M.R., Calaza C., Lamas D., Fonseca L., Fraigi L., Electrical transport properties of V_2O_5 thin films obtained by thermal annealing of layers grown by RF magnetron sputtering at room temperature. Thin Solid Films. 2015;**589**:730–734. DOI: 10.1016/j.tsf.2015.06.048

[46] Emin D., David E., Holstein T., Studies of small-polaron motion IV. Adiabatic theory of the Hall effect. Annals of Physics. 1969;**53**(3):439–520. DOI: 10.1016/0003-4916(69)90034-7

[47] Holstein T., Studies of polaron motion: Part I. The molecular-crystal model. Annals of Physics. 1959;**8**(3):325–342. DOI: 10.1016/0003-4916(59)90002-8

[48] Murawski L., Chung C.H. and Mackenzie J.D., Electrical properties of semiconducting oxide glasses. Journal of Non-Crystalline Solids. 1979;**32**(1):91–104. DOI: 10.1016/0022-3093(79)90066-8

[49] Cohen M., Review of the theory of amorphous semiconductors. Journal of Non-Crystalline Solids. 1970;**4**:391–409. DOI: 10.1016/0022-3093(70)90068-2